# RESEARCH ARTICLE

**Key Points:**
- Amplified anticyclonic ice drift in the 2000s compared to the 1980s/1990s
- Strongest drift curl trend in autumn, associated with increased ice export out of the southern Beaufort Sea
- Limited wind trends suggest other processes driving the enhanced Beaufort Gyre ice circulation

**Supporting Information:**
- Supporting Information S1
- Figure S1
- Figure S2
- Figure S3

**Correspondence to:**
A. A. Petty,
alek.a.petty@nasa.gov

# Sea ice circulation around the Beaufort Gyre: The changing role of wind forcing and the sea ice state

Alek A. Petty[1,2], Jennifer K. Hutchings[3], Jacqueline A. Richter-Menge[4], and Mark A. Tschudi[5]

[1]Earth System Science Interdisciplinary Center, University of Maryland, College Park, Maryland, USA, [2]Cryospheric Sciences Laboratory, NASA Goddard Space Flight Center, Greenbelt, Maryland, USA, [3]College of Earth, Ocean and Atmosphere, Oregon State University, Corvallis, Oregon, USA, [4]Cold Regions Research and Engineering Laboratory, Hanover, New Hampshire, USA, [5]Colorado Center for Astrodynamics Research, University of Colorado, Boulder, Colorado, USA

**Abstract** Sea ice drift estimates from feature tracking of satellite passive microwave data are used to investigate seasonal trends and variability in the ice circulation around the Beaufort Gyre, over the multidecadal period 1980–2013. Our results suggest an amplified response of the Beaufort Gyre ice circulation to wind forcing, especially during the late 2000s. We find increasing anticyclonic ice drift across all seasons, with the strongest trend in autumn, associated with increased ice export out of the southern Beaufort Sea (into the Chukchi Sea). A flux gate analysis highlights consistency across a suite of drift products. Despite these seasonal anticyclonic ice drift trends, a significant anticyclonic wind trend occurs in summer only, driven, in-part, by anomalously anticyclonic winds in 2007. Across all seasons, the ice drift curl is more anticyclonic than predicted from a linear relationship to the wind curl in the 2000s, compared to the 1980s/1990s. The strength of this anticyclonic ice drift curl amplification is strongest in autumn and appears to have increased since the 1980s (up to 2010). In spring and summer, the ice drift curl amplification occurs mainly between 2007 and 2010. These results suggest nonlinear ice interaction feedbacks (e.g., a weaker, more mobile sea ice pack), enhanced atmospheric drag, and/or an increased role of the ocean. The results also show a weakening of the anticyclonic wind and ice circulation since 2010.

## 1. Introduction

The Beaufort Gyre (BG) is a prominent anticyclonic circulation feature and freshwater reservoir within the Arctic Ocean, and is thought to play a significant role in regulating Arctic climate variability [*Aagaard and Carmack*, 1989; *Proshutinsky et al.*, 2002, 2009]. Sea ice variability within the BG region (shown in Figure 1) contributes to interannual variations in the Arctic sea ice cover [e.g., *Rigor et al.*, 2002], with the record sea ice minimum observed in 2012 thought to be driven, in-part, by significant ice reduction within the BG [*Parkinson and Comiso*, 2013; *Krishfield et al.*, 2014]. The mean September sea ice extent for the Arctic and BG region is shown in Figure 2. The ice and ocean circulation within the BG region is driven by a long-term annual mean sea level pressure high over the northern Beaufort Sea (the Beaufort High). The anticyclonic winds associated with this high-pressure system set the sea ice in motion, and the region accumulates freshwater through Ekman convergence and the subsequent downwelling of surface waters (a "spin-up" of the gyre).

Variability in the BG ice circulation has been attributed to variability in the Beaufort High, as described by the Arctic Oscillation (AO) [*Rigor et al.*, 2002]. In the 1980s/1990s, negative phases of the AO, which resulted in a strong and persistent Beaufort High, favored recirculation of thick, multiyear (MY) ice in the Arctic [*Rigor and Wallace*, 2004]. Since the late 1990s, there has been an increased import of young ice from the neighboring Chukchi Sea and a stronger poleward ice drift in summer, reducing the recirculation of ice within the Beaufort and Chukchi seas [*Hutchings and Rigor*, 2012]. These changes in ice dynamics combined with increased thermodynamic ice loss [*Kwok and Cunningham*, 2010; *Perovich et al.*, 2008, 2011] have reduced the survivability of ice within the Beaufort Sea, making this region a sink of MY ice [*Kwok and Cunningham*, 2010; *Maslanik et al.*, 2011]. Despite a record low AO index in winter 2010, the ice drifted further south into the Chukchi Sea and melted out before recirculating back into the Beaufort Sea, suggesting a loss of correlation between summer ice extent and the AO in recent years [e.g., *Stroeve et al.*, 2011; *Hutchings and Rigor*, 2012]. This provides further evidence to the claim that the AO is no longer a reliable indicator of Arctic
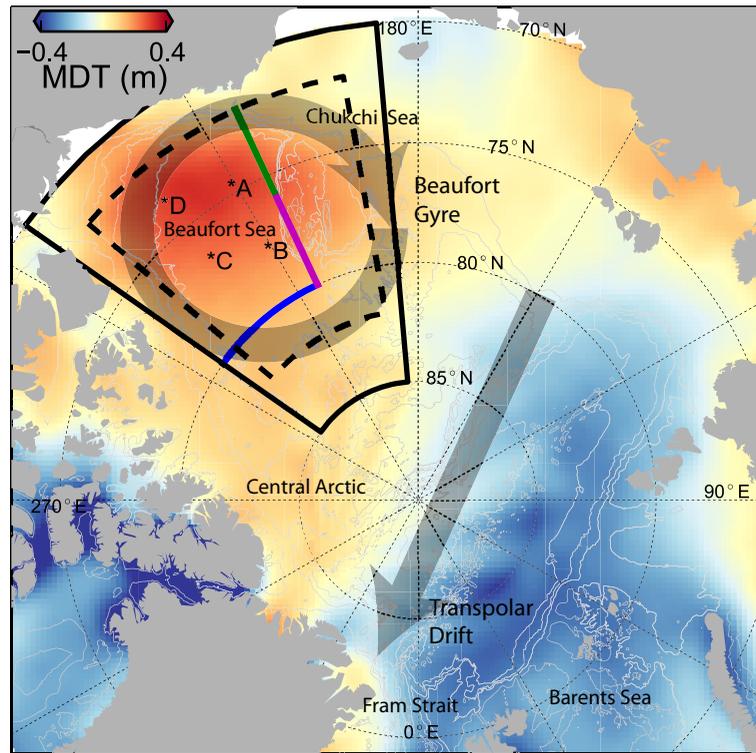
**Figure 1.** The mean (2003–2009) dynamic topography (MDT) of the Arctic Ocean derived from satellite altimetry [*Farrell et al.*, 2012], with the dark grey arrows broadly representing the mean circulation of the Beaufort Gyre and Transpolar Drift. The colored lines indicate the ice flux gates at (155°W/72°N–76°N, green), (155°W/76°N–80°N, magenta), and (125°W–155°W/80°N, blue). The black box (72°N–82°N/ 130°W–170°W, dashed line) indicates the region over which the ice drift curl was calculated, and the black box (70°N–85°N/125°W–175°W, solid line) indicates the region over which the wind curl and ice concentration/extent/thickness were calculated. The light grey lines are bathymetry contours, taken from the IBCAOv3 data set [*Jakobsson et al.*, 2012]. The letters (A–D) indicate the locations of the BGEP moorings [*Krishfield et al.*, 2014] used to calculate the mean ice thickness within the Beaufort Gyre (in Figure 3).

atmosphere/ice circulation variability [e.g., *Maslanik et al.*, 2007]. A more detailed investigation into the atmospheric circulation is therefore suggested when assessing variability in the dynamical forcing of the Arctic ice pack and ice circulation in the BG.

Estimates of ice thickness from the Pan-Arctic Ice-Ocean Modeling and Assimilation System (PIOMAS) [*Schweiger et al.*, 2011] and observations of ice draft [*Krishfield et al.*, 2014] and thickness (*Richter-Menge and Farrell* [2013], analysis extended to 2014) suggest a decrease in the thickness of ice in the BG region,
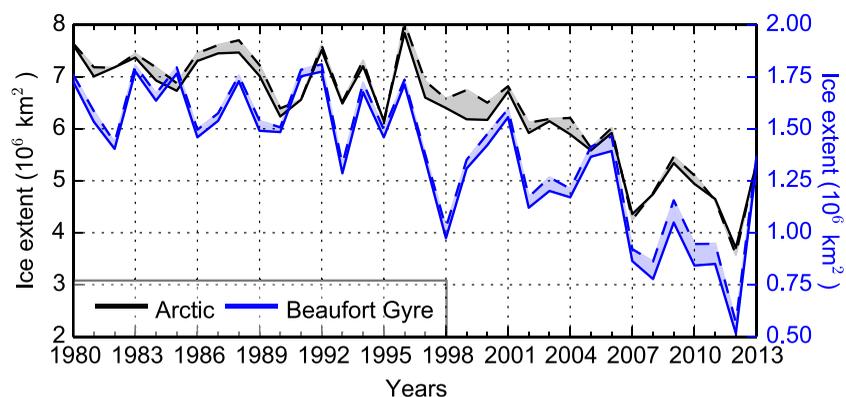


**Figure 2.** September mean sea ice extent of the Arctic (black) and Beaufort Gyre region (blue). The solid (dashed) line on either side of the color shading is the ice extent calculated using the NASA Team (Bootstrap) processing of passive microwave data. The Beaufort Gyre region is defined by the solid black box in Figure 1.
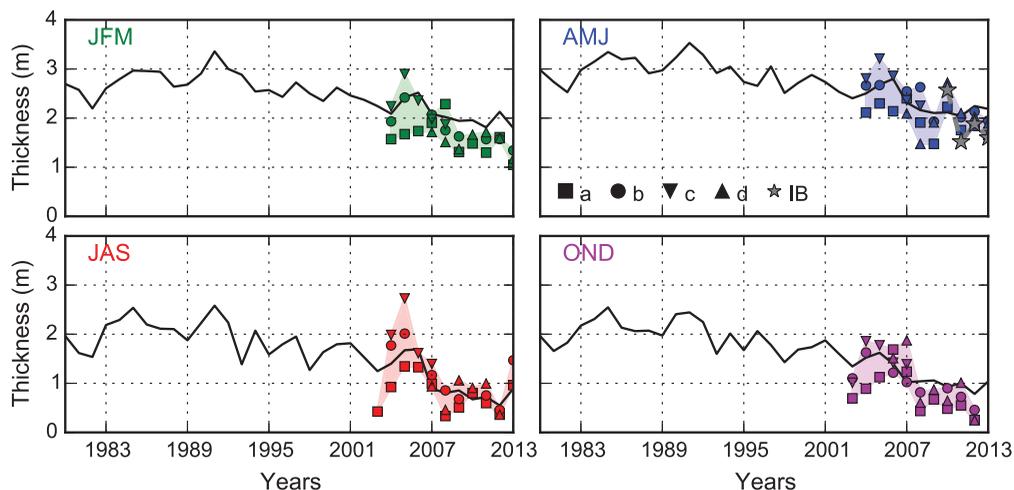
**Figure 3.** Seasonal mean ice thickness within the Beaufort Gyre region. The black line indicates the mean seasonal ice thickness within the Beaufort Gyre region (solid black box in Figure 1) estimated from PIOMAS data (1980–2013). The colored markers and shading indicate the regional variability of ice thickness estimated from the four separate BGEP moorings (a–d) (2003–2011). The gray stars (and gray dashed lines) in the top right plot indicate the mean ice thickness within the Beaufort Gyre region calculated from IceBridge observations in March/April (2010–2014). JFM: January–March, AMJ: April–June, JAS: July–September, and OND: October–December.

associated with a loss of MY ice. The seasonal ice thickness estimates are shown in Figure 3 and are described in more detail in section 2.3. Coinciding with this loss of MY ice is a significant decline in the summer (July–September) and autumn (October–December) ice concentration, as shown in Figure 4. The Arctic concentration trends, shown in Figure 5, demonstrate that the summer concentration decline observed over much of the southwestern Beaufort Gyre region is amongst the strongest seasonal decline observed across the entire Arctic. Together with these observed changes in sea ice, the liquid freshwater content (FWC) of the BG has increased over recent decades [*McPhee et al.*, 2009; *Rabe et al.*, 2011], contributing to an increased doming of the BG [*Giles et al.*, 2012].

The relative contributions to changes in the BG FWC from Ekman convergence, river runoff and other processes including sea ice melt, is still an active area of discussion [e.g., *Yamamoto-Kawai et al.*, 2009; *Morison et al.*, 2012; *Krishfield et al.*, 2014]. *McPhee* [2013] found increased Ekman convergence in the BG in late
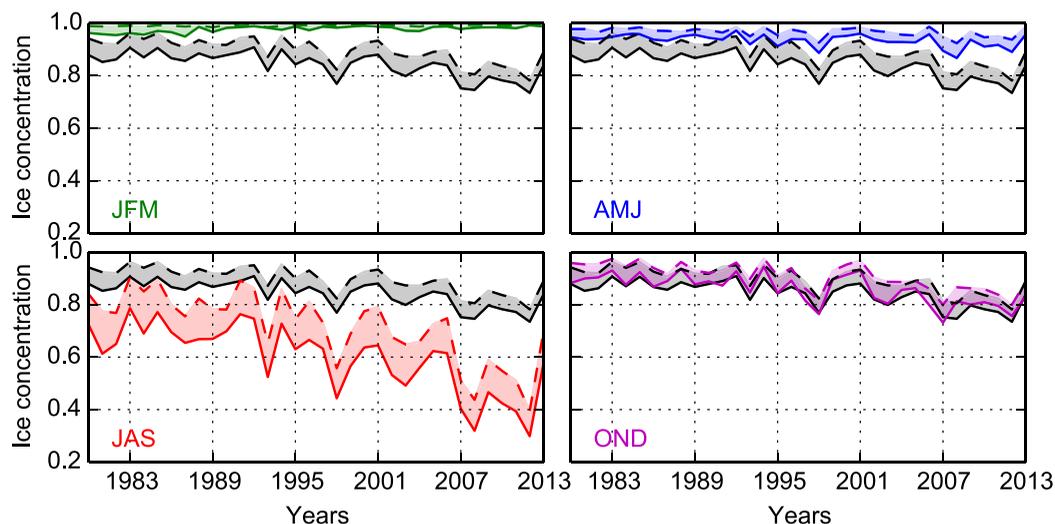


**Figure 4.** Seasonal (separate plots and colors) and annual mean (black in all plots) 1980–2013 ice concentration within the Beaufort Gyre region (solid black box in Figure 1). The solid (dashed) line either side of the color shading is the ice concentration calculated using the NASA Team (Bootstrap) processing of passive microwave data.
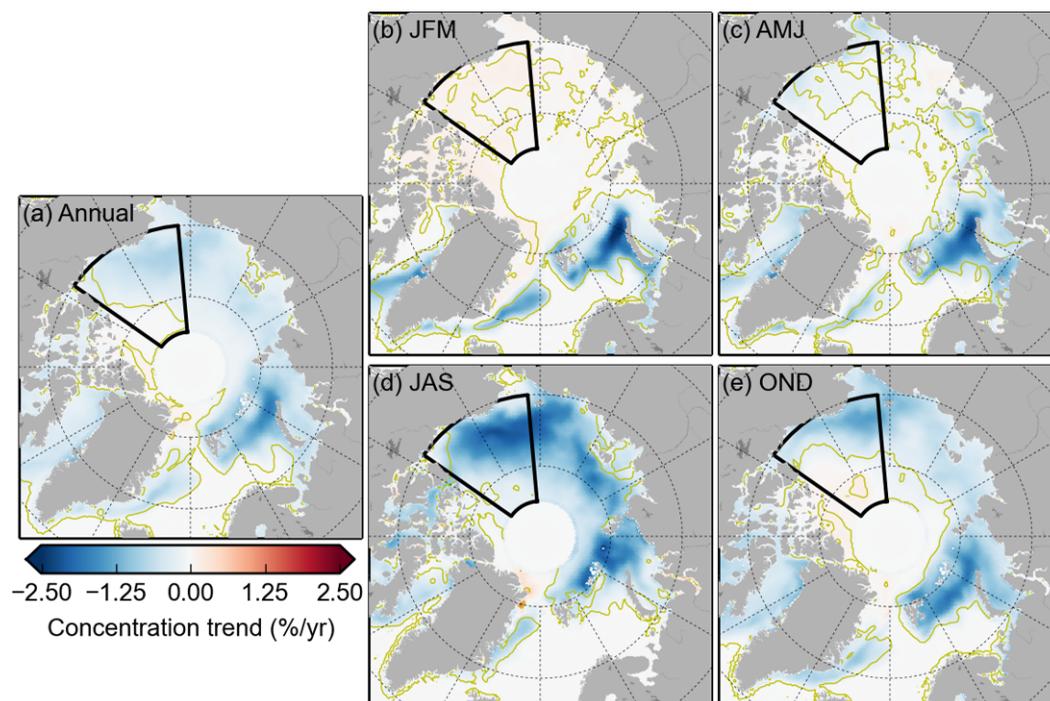
**Figure 5.** (a) Annual and (b–e) seasonal ice concentration trend over the Arctic from 1980–2013, estimated from the NASA Team processing of passive microwave data. Note that a "pole hole" exists in the concentration data above 85°N. The yellow contour indicates concentration trends significant at 95%. The solid black box is used to define the Beaufort Gyre region, as in Figure 1.

summer (September/October) linked to increased wind forcing (August–October, 1980–2011), while *Yang* [2009] found increased Ekman convergence through autumn (October–December, 1979–2006), which he linked to enhanced ice circulation, independent of the wind forcing. Similarly, *Giles et al*. [2012] showed that on an annual time scale (1995–2010), the wind forcing was unable to explain the increased doming of the BG, suggesting instead that changing sea ice characteristics may be altering the effective momentum transfer between the atmosphere and ocean.

Arctic sea ice drift has increased over recent decades, which has been linked to the thinning [*Spreen et al.*, 2011] and weakening [*Rampal et al.*, 2009] sea ice cover, over and above the smaller (to negligible) trends in wind forcing [*Hakkinen et al.*, 2008; *Kwok et al.*, 2013]. In the recent modeling study of *Martin et al.* [2014], the momentum transfer through sea ice increased as a function of ice concentration (up to 80–90%) due to enhanced wind drag over the rougher ice surface, but decreased at higher ice concentrations due to increased ice-ice interactions. The reductions of sea ice concentration in the BG region through autumn (described above) could therefore be pushing the region toward a state that optimizes the transfer of momentum between the atmosphere and ocean. In the study of *Martin et al.* [2014], the impact from variable atmosphere-ice/ice-ocean drag coefficients was neglected. These drag coefficients vary temporally and spatially and thus provide a further influence over the effective momentum transfer through the ice pack [e.g., *Guest and Davidson*, 1991; *Lupkes et al.*, 2012; *Tsamados et al.*, 2014]. Geostrophic ocean current increases caused by the increased doming of the BG are also thought to be increasing ice drift through reduced ice-ocean stress, especially along the southern periphery of the BG [*McPhee*, 2013].

Our study builds on earlier research demonstrating enhanced Arctic sea ice drift [e.g., *Spreen et al.*, 2011; *Kwok et al.*, 2013] by utilizing several approaches that collectively provide a more detailed understanding of the BG circulation changes. These include: (i) a seasonal and regional analysis of wind forcing, ice circulation, and ice state changes within the BG, as high seasonal variability in the BG ice and ocean circulation has been previously demonstrated [e.g., *Yang*, 2009; *Proshutinsky et al.*, 2009; *Hutchings and Rigor*, 2012; *Krishfield et al.*, 2014]; (ii) an analysis of the wind field/ice drift curl to be consistent with the results of previous studies investigating the BG forcing [e.g., *Yang*, 2009; *Giles et al.*, 2012]; and (iii) the analysis of several different wind/sea ice drift data sets to increase confidence in our results, considering the uncertainties in

Arctic wind [*Lindsay et al.*, 2014] and ice drift [*Sumata et al.*, 2014] estimates. We analyze a multidecadal (1980–2013) time series of the wind and ice circulation around the BG, covering the long-term downward trend in sea ice extent within the Arctic and BG region, the drastic sea ice declines observed in 2007/2008, and the strong increase in extent/concentration in 2013. A detailed discussion surrounding the changes to the sea ice state is provided to increase our understanding of the magnitude and timing of the changes taking place within this dynamic system.

The paper is organized as follows: section 2 presents the data sets used in this study; section 3 discusses the methods employed to investigate the changing ice circulation, wind forcing, and sea ice state; section 4 presents results from our various analyses; section 5 discusses possible causes of a changing sea ice circulation; and conclusions are given in section 6.

## 2. Data

### 2.1. Sea Ice Drift

The Polar Pathfinder daily 25 km EASE-grid sea ice motion vectors, version 2 [*Fowler et al.*, 2013] available at the National Snow and Ice Data Center (NSIDC), referred to herein as NSIDC/PP, provide sea ice drift vectors for all months of the year from 1980 to 2013 across the entire Arctic basin. The drift vectors are calculated from feature tracking of a variety of passive microwave satellite sensors, buoy drift estimates from the International Arctic Buoy Programme (IABP) and wind data from the National Centers for Environmental Prediction (NCEP)-National Center for Atmospheric Research (NCAR) Reanalysis. The sea ice drift is calculated using a cross-correlation technique applied to sequential, daily satellite images acquired by the passive microwave sensors. These motion vectors are blended via optimal interpolation with the buoy drift vectors and NCEP/NCAR wind fields to produce a daily sea ice motion product [*Fowler et al.*, 2003]. The interpolation helps minimize the drift error, which is recorded for each vector with a quality flag, as described in the associated documentation (nsidc.org/data/docs/daac/nsidc0116_icemotion.gd.html). Note that a 1 day lag is used for the cross correlation after July 1987, but a 2 day lag was required from November 1978 to July 1987, before the Scanning Multichannel Microwave Radiometer (SMMR) was replaced with the launch of the Special Sensor Microwave Imager (SSM/I). We choose to mask the data based on the flags indicating the vector's proximity to the coast (flagged if the data is within 25 km of the coast) and the proximity to the nearest raw input data source prior to interpolation (flagged if the nearest raw data source is greater than 1250 km away). We choose not to mask based on the estimated variance of the drift vectors as an uncertain drift is assumed to be more accurate than assuming there is no ice (or ice flux) at that location. Note that if the ice concentration falls below 15%, the ice parcel is no longer tracked. Errors in the feature tracking of ice parcels also increase during summertime, when melt ponds can be misinterpreted by the passive microwave sensor as open water. Advanced Very High Resolution (AVHRR) imagery is incorporated into the NSIDC/PP product in an attempt to correct this issue, but the prevalence of clouds limits its effectiveness. Daily, weekly, monthly, and annual ice drift means are provided by the NSIDC. We use the daily drift data in this study, as we square the drift in calculating the ice drift curl. The daily data also provide flexibility in the number of valid daily drift vectors we deem sufficient to calculate a monthly estimate. The vectors are provided on an Equal Area Scalable Earth (EASE) grid with 25 km horizontal resolution.

Due to these potentially large uncertainties in the calculation of ice drift from passive microwave feature tracking, especially in regions of low ice concentration and thickness (as discussed in more detail by *Sumata et al.* [2014]), we compare the NSIDC/PP analysis with drift data produced by the Centre ERS d'Archivage et de Traitement (CERSAT), part of the Institut Français de Recherche pour l'Exploitation de la Mer (IFREMER). CERSAT provides a number of ice drift products through the merging of passive microwave brightness data with scatterometry data from the National Aeronautics and Space Administration (NASA) Ku-band Quick Scatterometer (QuikSCAT, 1999–2009), referred to herein as CSAT/QS, and the European Space Agency (ESA) C-band Advanced Scatterometer (ASCAT, 2008–2013), as described in *Girard-Ardhuin and Ezraty* [2012]. The use of scatterometers is thought to improve the detection of ice drift during ice transitions (freeze/melt periods) as they are less sensitive to surface wetness than passive microwave sensors [*Girard-Ardhuin and Ezraty*, 2012; *Sumata et al.*, 2014]. A cost-function analysis is used to determine which combination of the various input vectors are used in the merged product (at each location). CERSAT provide data using both a 3 and 6 day lag in the tracking of ice displacement (as well as monthly mean data sets using

predominantly the 6 day lag data). The 6 day lag is expected to provide better estimates of slow ice drift as it provides more time for the ice parcel to move a noticeable distance, while the 3 day lag is more appropriate for faster drifts as it increases the resolution of the ice parcel path, an important issue when analyzing the curl of the ice drift. We therefore mainly focus on the 3 day data (referred to herein as CSAT/AS-3) but choose to show the results of 6 day data (referred to herein as CSAT/AS-6) to demonstrate the impact from this choice of lag time. Note that both lag times are longer than the 1 day lag used predominantly in the NSIDC/PP product. The CERSAT products are masked if they fail to pass a number of tests (e.g., spatial coherence, correlation with surface winds) as described in the documentation (ftp://ftp.ifremer.fr/ifremer/cersat/products/gridded/psi-drift/documentation/merged.pdf).

From the daily NSIDC and quasi-daily CERSAT data, we produce monthly mean drift vectors using all daily/quasi-daily drift data available within that month. At least 15 days of valid drift data are needed to produce a monthly mean drift estimate. This is less than the NSIDC/PP monthly product (20 days) and differs from the CERSAT monthly products (which combines consecutive 6 day lag drift vectors), allowing us to increase the amount of data available within this seasonally transitioning sea ice region. Seasonal (3 month) data sets are produced through the averaging of these monthly data.

### 2.2. Winds

The sparsity of near-surface wind observations over the Arctic limits our ability to assess the accuracy of the various atmospheric reanalysis products available. *Lindsay et al.* [2014] recently compared several reanalyses products over the Arctic to available observations. However, the wind observations were predominantly over the central Arctic Ocean and there was no assessment of the wind curl/vorticity. To increase our confidence in the estimated wind forcing over the BG, we therefore compare wind data from three separate reanalyses: (i) the NCEP/NCAR Reanalysis 2 (NCEP-R2) [*Kanamitsu et al.*, 2002], (ii) the European Centre for Medium-Range Weather Forecasts (ECMWF) Interim Reanalysis (ERA-I) [*Dee et al.*, 2011], and (iii) the Japanese 55 year Reanalysis Project (JRA-55) produced by the Japanese Meteorological Agency (JMA) [*Ebita et al.*, 2011], which all provide daily data over the entire temporal domain of the NSIDC/PP data set. Several other reanalysis products are available (see *Lindsay et al.* [2014] for a summary), however, we choose to limit our study to these three commonly used reanalyses which cover the entire 1980–2013 temporal range. Note that these three reanalyses (JRA-25 not JRA-55) also provided the strongest agreement in Arctic sea level pressure (smallest deviations from the seasonal cross-reanalysis median) in the study of *Lindsay et al.* [2014].

### 2.3. Sea Ice Concentration and Thickness

To assess the concentration of ice within the BG region, we use both the NASA Team [*Cavalieri et al.*, 1996] and Bootstrap [*Comiso*, 2000] processing of passive microwave satellite data. These data sets are both made available through the NSIDC on a polar stereographic grid (25 km horizontal resolution) covering the entire 1980–2013 temporal range of this study. The NASA Team concentration data are used when combining with the drift data sets to produce estimates of ice area import/export (as discussed in the following section).

Ice thickness observations within the BG region are temporally and spatially sparse. Here we utilize several different data sets, including the 2003–2013 (annual) ice draft estimates derived from Upward Looking Sonar (ULS) data from four different moorings deployed during the Beaufort Gyre Exploration Project (BGEP) [*Krishfield et al.*, 2014] (see Figure 1 for locations of the moorings). We calculate seasonal mean ice drafts from the daily binned ULS data for each of the four moorings where there is more than 60 days of data available within the season. We follow the approach of *Rothrock et al.* [2008] and *Lindsay and Schweiger* [2015] in converting ice draft to ice thickness using fixed values for the ice and snow density. The ice thickness can be related to ice draft as $h_i = 1107 h_d - f(m)$, where $h_d$ is the observed ice draft and $f(m)$ is the seasonal mean ice equivalent of snow on the ice surface, estimated by *Rothrock et al.* [2008] using the snow climatology of *Warren et al.* [1999]. Decreases in Arctic snow depth [*Webster et al.*, 2014] suggest that these estimates of $f(m)$ may be biased high, making our $h_i$ estimates potentially biased low. These results are compared with the 2009–2014 (March/April) ice thickness estimates from NASA Operation IceBridge data (*Richter-Menge and Farrell* [2013], analysis extended to 2014). Note that the Beaufort and Chukchi Sea region defined in *Richter-Menge and Farrell* [2013] extends further west and south (170°W–120°W and 69°N–79°N) than our BG study region and the 2009/2011 data are only sparsely sampled within this region, so less

weight should be given to the comparison in those years. To provide an estimate of the BG ice thickness covering the entire temporal range of this study (1980–2013), seasonal estimates of the BG ice thickness from the Pan-Arctic Ice-Ocean Modeling and Assimilation System (PIOMAS, v2.1) [*Schweiger et al.*, 2011] are presented. PIOMAS is an ice-ocean model, producing ice thickness estimates constrained predominantly by the assimilation of sea ice concentration and sea surface temperature.

## 3. Methods

### 3.1. Flux Gate Analysis

To investigate the circulation of ice around the BG, two zonal flux gates (along 155°W) are used to highlight the export of ice from the southern Beaufort Sea into the neighboring Chukchi Sea (72°N–76°N) and the transport between the central BG region and the western periphery of the BG, north of the Chukchi Sea (76°N–80°N). One meridional flux gate (125°W–155°W along 80°N) is used to highlight the import of ice into the Beaufort Sea from the central Arctic (see colored lines in Figure 1).

The monthly drift vectors produced from the daily drift data sets and the monthly NASA Team sea ice concentration estimates are interpolated onto the flux gates at a spacing of roughly 20 km to produce estimates of the total ice area transport through the two zonal flux gates and one meridional flux gate as

$$F_u = \sum_{i=1}^{N} A_i u_i \Delta x_u T_s \tag{1}$$

$$F_v = \sum_{i=1}^{N} A_i v_i \Delta x_v T_s \tag{2}$$

where $A_i$ is the ice concentration at a given point $i$ along the gate, $u_i$ and $v_i$ are the zonal and meridional components of ice drift, respectively, $N$ (=20) is the number of interpolation points along the flux gate, $\Delta x_u$ and $\Delta x_v$ are the spacings between the interpolation points along the zonal and meridional flux gates, respectively, and $T_s$ is the number of seconds in a month used to convert the fluxes into an area transport (import/export). Note that for the NSIDC/PP product, a further calculation was carried out without ice concentration ($A$) included to assess the impact of changing ice concentration on the ice transport. The area transports were summed together within each season to produce the seasonal area transports through each flux gate, as shown in Figure 6.

### 3.2. Atmosphere-Ice-Ocean Momentum Transfer

While acknowledging known complexities in the exchange of momentum between the ice and ocean [e.g., *McPhee*, 2012], we follow several other studies [e.g., *Hibler and Bryan*, 1987; *Martin et al.*, 2014] in assuming that the transfer of wind stress into the ocean through sea ice is given to a first-order approximation as

$$\tau_\mathbf{o} = \tau_\mathbf{a} + \mathbf{F_i} \tag{3}$$

where, following *Martin et al.* [2014], $\mathbf{F_i}$ represents the internal stresses within the ice pack and the interaction between ice floes. Note that $\mathbf{F_i}$ mainly acts in the opposite direction to the wind stress and thus acts to reduce the transfer of momentum through the ice pack [e.g., *Hibler*, 1979]. We have ignored terms in the sea ice momentum balance due to the Coriolis and sea surface tilt forces as they are small on seasonal time scales [e.g., *Steele et al.*, 1997]. The atmosphere-ice $\tau_\mathbf{a}$ and ice-ocean $\tau_\mathbf{o}$ stresses can be expressed using quadratic boundary layer drag laws [e.g., *Brown*, 1980; *McPhee*, 1982] as

$$\tau_\mathbf{a} = C_a \rho_a |\mathbf{U_a}| \mathbf{U_a} \tag{4}$$

$$\tau_\mathbf{o} = C_o \rho_w |\mathbf{u} - \mathbf{U_o}| [\mathbf{u} - \mathbf{U_o}] \tag{5}$$

where $\mathbf{u}$ is the ice velocity, $\mathbf{U_a}$ is the near-surface (10 m) wind velocity (which is assumed to be much larger than the ice velocity), $\mathbf{U_o}$ is the near-surface ocean current, and $C_a$ ($C_o$) is a bulk drag coefficient over (under) the sea ice surface.

To provide insight into the strength of the atmosphere-ice coupling, we adopt a highly idealized model of sea ice momentum transfer by assuming the ice interaction force and drag coefficients to be constant in
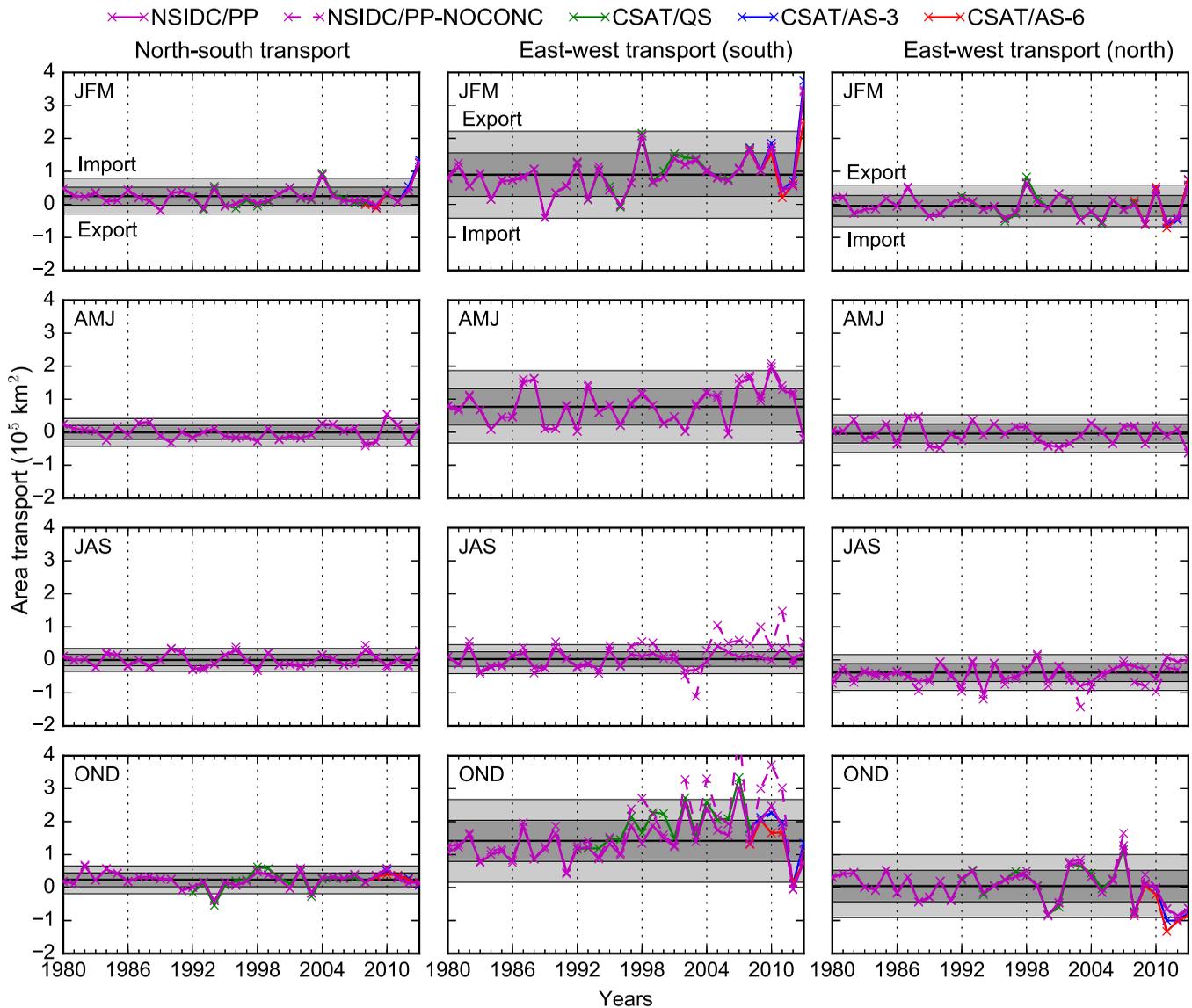
**Figure 6.** Seasonal mean (top to bottom) ice area transport through the three flux gates shown in Figure 1 (left to right) calculated from the NSIDC/PP (1980–2013, magenta), CSAT/QS (1992–2008, green), CSAT/AS-6 (2008–2013, red), and CSAT/AS-3 (2008–2013, blue) drift data sets combined with NASA Team ice concentration data. CSAT area transports are only shown in winter (JFM) and autumn (OND) due to the limited availability of drift data within spring (AMJ) and summer (JAS). The dark (light) grey shading represents ±1(2) standard deviations from the mean of the NSIDC/PP results (black line). The dashed magenta line shows the area transport from the NSIDC/PP product excluding ice concentration weighting (NSIDC/PP-NOCONC). Import (export) refers to ice entering (leaving) the Beaufort Gyre region (Figure 1) through the respective flux gate.

space and time, and neglect near-surface ocean currents. We acknowledge that these quantities are, in-fact, spatially and temporally variable [e.g., *Thorndike and Colony*, 1982; *Guest and Davidson*, 1991; *Steele et al.*, 1997; *Feltham*, 2008; *Lupkes et al.*, 2012; *Tsamados et al.*, 2014]. However, this idealized approach is taken to understand if and when this simple model may be appropriate, and when the presence and/or variability in the neglected components of the force balance may be significant. Using these assumptions, we can combine the two different expressions for $\tau_o$ in equations (3) and (5), and take the curl of both sides to produce a simple linear relationship between the wind and ice drift circulation as

$$\nabla\times\mathbf{u}|\mathbf{u}| \propto \nabla\times\mathbf{U_a}|\mathbf{U_a}|. \qquad (6)$$

The vertical components of the wind field curl and ice drift curl (scalar quantities) are used in a linear regression analysis. Deviations from the linear relationship suggest either a loss of correlation or indicate nonlinear coupling between the wind and ice circulation, which could be caused by variability in the ice interaction force, the atmospheric/oceanic drag coefficients, ocean currents, and/or some other process not accounted

for in this model. Note that we do not attempt to accurately quantify ice-ocean stress and Ekman pumping, as was carried out in previous studies of the BG [e.g., *Yang*, 2009; *McPhee*, 2013].

We analyze the vertical component of the wind field curl and ice drift curl as

$$(\nabla \times |\mathbf{u}|\mathbf{u}) \cdot \mathbf{z} = \frac{\partial(|\mathbf{u}|u_y)}{\partial x} - \frac{\partial(|\mathbf{u}|u_x)}{\partial y} \tag{7}$$

$$(\nabla \times |\mathbf{U_a}|\mathbf{U_a}) \cdot \mathbf{z} = \frac{\partial(|\mathbf{U_a}|U_y)}{\partial x} - \frac{\partial(|\mathbf{U_a}|U_x)}{\partial y} \tag{8}$$

where $U_x/U_y$ and $u_x/u_y$ are the $x/y$ components of the daily wind and ice velocities (discussed in the previous section) and $\mathbf{z}$ is a unit vertical vector. The wind and ice drift vectors were projected onto a 100 km polar stereographic grid using a linear interpolation scheme before calculating the curl for consistency amongst the different products and to better represent the broader regional wind and ice drift circulation over the BG. Monthly means are produced from the daily wind field/ice drift curls, from which seasonal means are calculated. The calculation of a monthly mean ice drift curl requires more than 15 days of valid drift data within that month. Negative (positive) values of the ice drift/wind field curl correspond to an anticyclonic (cyclonic) circulation. While we acknowledge variability in the size and location of the BG ice-ocean circulation [e.g., *Rigor et al.*, 2002; *Proshutinsky et al.*, 2002], the seasonal ice drift/wind field curls are averaged over a constant BG study region (shown in Figure 1) to enable temporal comparisons of these variables [e.g., *Proshutinsky et al.*, 2009]. Note that we use a larger wind field curl study region compared to the ice drift curl study region, to include storm tracks entering the Arctic Ocean through the Chukchi Sea [e.g., *Screen et al.*, 2011] and to better represent the broader region influenced by the Beaufort High [e.g., *Serreze and Barrett*, 2010]. This is a similar approach to other recent studies investigating the BG ice/atmosphere circulation [e.g., *Asplin et al.*, 2009]. By considering the relationship between the wind field and ice drift curl across different seasons, we can explore whether any specific seasonal sea ice changes could be contributing to a nonlinear response of ice drift to the given wind forcing. For example, some seasons may be more responsive to changes in thickness and/or concentration depending on the mean seasonal sea ice state (e.g., the ice may simply remain in a state of free drift in summer, despite decreases in ice concentration).

## 4. Results

### 4.1. Ice Circulation Around the Beaufort Gyre

Figure 6 shows the seasonal transport of ice through the three different flux gates using the NSIDC/PP and CERSAT drift products. The same figure with variable $y$ axes is given as a supporting information figure (Figure S1) to more clearly demonstrate the differences between the products where the fluxes are low. Supporting information Figure S1 also includes a calculation of area transport with the NSIDC/PP drift combined with the Bootstrap, instead of NASA Team ice concentration data. The results demonstrate a strong agreement between the products across the meridional (80°N/125°W–155°W) and northern zonal flux gates (76°N–80°N/155°W) in all seasons. There is also a strong agreement between the products across the southern zonal flux gate (72°N–76°N/155°W) in winter (January–March, JFM), where ice concentrations are high and/or drift speeds are low. The products show small differences through the southern zonal flux gate (72°N–76°N/155°W) in autumn (October–December, OND), where the transport is high and ice concentration is more variable. This result agrees with the recent conclusions of *Sumata et al.* [2014], who compared the NSIDC/PP and CERSAT products with two other passive microwave sea ice drift products in the Arctic and drift estimates from the IABP, demonstrating a similar link to this study between drift speed, ice concentration, and drift uncertainty. The NSIDC/PP estimated area transport through the southern zonal flux gate in autumn tend to be lower in magnitude than the CERSAT transports, although there is still strong agreement in the pattern of interannual variability. This increases our confidence in estimating the trend and variability in the ice circulation around the BG from the longer NSIDC/PP time series. The lack of complete spring (April–June, AMJ) and summer (July–September, JAS) data in the CERSAT products prevent a comparison in these seasons. Note that CERSAT do produce drift estimates in April, May, and September (outside of the melt season), but this was insufficient to produce a seasonal mean that could be compared to the NSIDC/PP estimates.

The export through the southern zonal flux gate in autumn shows the strongest trend of all seasons/flux gates. Here the estimated export becomes anomalously high in the 2000s ($\sim2.5 \times 10^5$ km$^2$) compared to the 1980s/1990s ($\sim1 \times 10^5$ km$^2$), peaking in 2007, before reducing to an anomalously low area transport with no clear import or export in 2012 ($\sim$2 SD below the mean). The area transport returns to a value more representative of the climatological mean in 2013. The CSAT/QS (1992–2008) results show a similar increase, while the two CSAT/AS (2008–2013) products corroborate the rapid decline in 2012 and small increase in 2013. A similar trend is not as apparent in winter, however, the export out of the southern Beaufort Sea is on average higher since the mid-1990s, including an anomalously strong export in 2013 ($\sim3 \times 10^5$ km$^2$). In summer, the ice shows no strong tendency between import or export out of the southern Beaufort Sea, except for the recent years of high nonconcentration weighted transport (dashed lines in Figure 6). This implies less concentrated summer ice is able to circulate faster around the southern Beaufort Sea, yet the area of ice being exported to the Chukchi Sea has not changed. Note that it is difficult to compare our results to those of *Kwok et al.* [2013] as they analyzed Arctic sea ice drift across different seasonal time periods (October–May and April–September) in 9 year cycles. However, their results also show an increasing westward ice drift through the southern Beaufort Sea in recent decades (from 1992 to 2009).

No clear trends are apparent in the export of ice through the northern zonal flux gate, although there is high interannual variability in the estimated area transport in autumn. The export was anomalously high in autumn 2007, coinciding with the high export out of the southern zonal flux gate. The area transports in autumn after 2010 were anomalously low (a net import of ice in these years). The increasing ice export out of the southern zonal flux gate combined with the relatively constant area transport through the northern zonal flux gate prior to 2007 indicate an increase in the anticyclonic ice drift through this period. Potential trends in the seasonal ice drift curl are investigated in the following section.

No clear trends are apparent in the import of ice through the meridional flux gate into the Beaufort Sea, although the results do indicate anomalously high imports in winter 2004 and 2013, spring 2010, and summer 2008.

Intuitively, we might expect a link between the import of ice from the north and export of ice to the east, due to the mean anticyclonic ice circulation in the region. This appears to be the case in 2013 when all the gates show anomalously high transports, indicating a large import of ice from the north and export to the east, but not in 2004 when the import through the meridional gate was anomalously high but the export out of the zonal gates was relatively low. It may be that the ice pack has become more mobile and/or the vertical redistribution of ice (through pressure ridging) may have reduced, strengthening this import/export connection. Further knowledge of the ice state variability is needed to investigate this idea in more depth. Analysis of the preliminary 2014 winter/spring NSIDC/PP data (not shown) demonstrates the return to more climatologically representative winter transports following the high transports (across all gates) in winter 2013. No anomalous transports were observed in spring 2014.

In general, the results suggest a tendency for increased ice loss from the Beaufort Sea since the 1980s, due primarily to increased ice export out of the southern Beaufort Sea into the Chukchi Sea in autumn. However, the ice circulation still appears able to revert back to a state that promotes ice retention, as was observed in 2012.

### 4.2. Correlation Between the Wind Field and Ice Drift Curl

Figure 7 shows the seasonal wind and drift curl over the BG. The only statistically significant trend ($>$90%) in the wind curl is during summer, with all three reanalyses showing a significant (92–97%) anticyclonic trend (more negative), mainly driven by the strong anticyclonic wind forcing throughout the 2000s. Note that removing 2007, a year of anomalously anticyclonic winds, decreased the significance of the anticyclonic wind trend in summer (83–93%). Maps of the seasonal wind curl trends from the three different reanalyses are provided in Figure 8, which show this significant anticyclonic wind trend in summer manifests across the northern Beaufort Sea and extends further northward into the central Arctic.

In contrast, the ice drift curl shows significant ($>$99%) trends of increasing anticyclonicity across all seasons. The strongest trend is in autumn ($6\times10^{-10}$ m s$^{-2}$yr$^{-1}$), despite the recent decrease (less anticyclonic) after 2010. Note that this autumn ice drift curl is roughly 6 times higher (more anticyclonic) in the late 2000s compared to the early 1980s. These results agree well with those of *Yang* [2009] while extending the time series beyond 2006, when the ice drift curl appears strongly amplified. These results also suggest that the
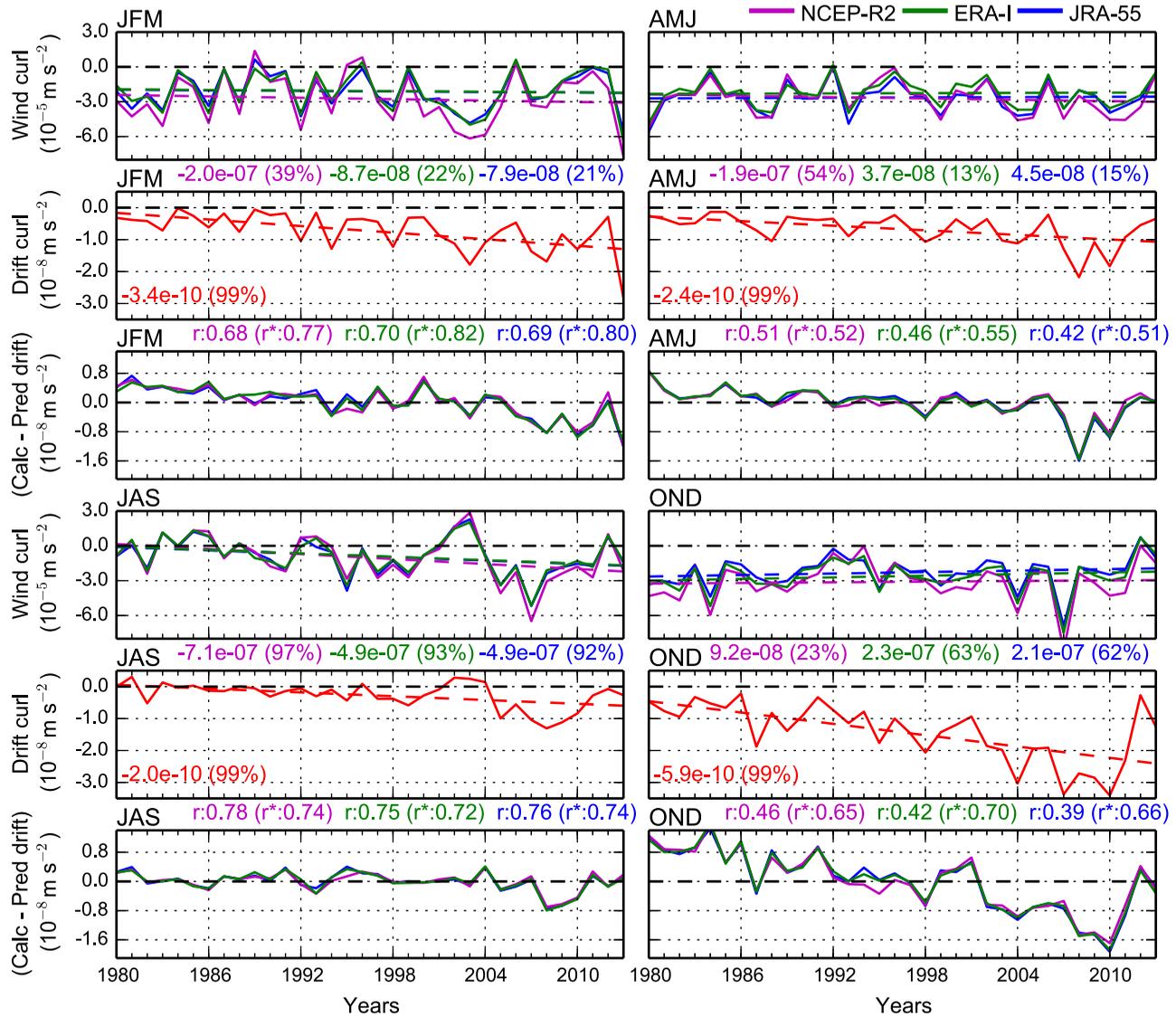
**Figure 7.** Seasonal mean 1980–2013 wind curl from ERA-I/NCEP-R2/JRA-55 (top plot in each quadrant), ice drift curl from NSIDC/PP (middle plot in each quadrant), and the anomaly between the calculated ice drift curl and the predicted drift curl assuming a linear relation between the wind and ice drift curl (bottom plot in each quadrant). The numbers between the top and middle plot in each quadrant indicate the linear wind curl trends (and significance) for the three reanalyses. The red numbers within the drift curl plots indicate the linear drift curl trend (and significance). Note that the trends are all in units of m s$^{-2}$ yr$^{-1}$. The numbers between the middle and bottom plot in each quadrant show the linear correlations (and detrended, r*, correlations) between the drift curl and the wind curl (from the three reanalyses). The wind curl (drift curl) is calculated within the solid (dashed) black box, as shown in Figure 1.

summer wind forcing and ice circulation around the BG in the late 2000s was a significant contributor to the net annual circulation, in contrast to the results shown by *Yang* [2009] for the period prior to 2007.

Note that, in Figure 7, we show only the ice drift curl derived from the NSIDC/PP product due to its longer (1980–2013) temporal range. However, the drift curl derived from the three CERSAT products (across their shorter temporal ranges), as well as maps of the seasonal drift curl trends from the NSIDC/PP data, are provided in Figure 9.

As demonstrated in Figure 9, the CSAT/QS drift curl shows strong agreement with NSIDC/PP in winter but gives a stronger anticyclonic drift curl and trend than NSIDC/PP in autumn. This suggests the NSIDC/PP results discussed here are likely to be conservative, especially in 2007 when CSAT/QS shows an anticyclonic drift roughly double that of the NSIDC/PP. To assess the impact on the results from the changing areal coverage of the ice pack (i.e., the reduced ice extent in the 2000s could bias the drift curl analysis to the northern Beaufort Sea), we also carry out the drift curl analysis with the NSIDC/PP monthly curl masked across all
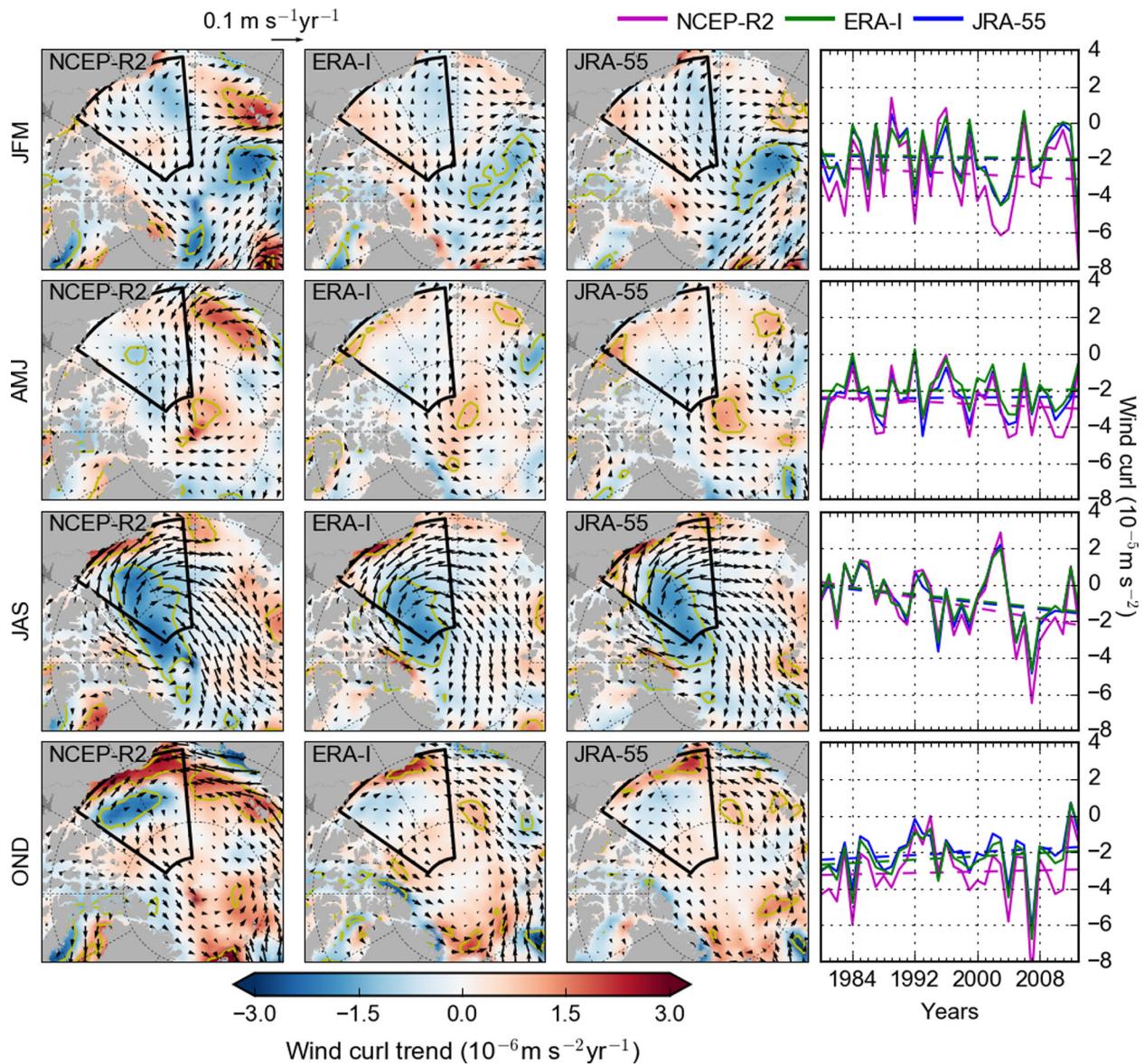
**Figure 8.** (left) Annual trend (1980–2013) in the seasonal mean wind field curl, based on the (left) NCEP-R2, (middle) ERA-I, and (right) JRA-55 reanalysis data. The yellow contour indicates wind curl trends significant at 95%. The arrows indicate trends in the wind vectors (every second vector shown). (right) Annual time series of the seasonal mean wind curl in the Beaufort Gyre region (within the solid black box, as in Figure 1).

years (NSIDC/PP-MASK in Figure 9) based on the minimum monthly areal coverage within the entire temporal range (1980–2013). This shows similar results to those discussed above, meaning the changes in ice circulation manifest broadly across the BG ice pack.

A linear regression between the wind and drift curl (Figure 7) shows the highest correlation in summer (r = 0.75–0.78) and winter (r = 0.68–0.70), but is considerably lower in spring (r = 0.42–0.51) and autumn (r = 0.39–0.46). To understand whether the seasonal ice drift and/or wind curl trends are reducing or increasing the strength of these correlations, we also provide detrended correlations (r*) in Figure 7. These show higher correlations in spring (0.51–0.55), winter (0.77–0.82), and autumn (0.65–0.70), when we see significant anticyclonic ice drift trends but no significant wind curl trends. The difference between the regular and detrended correlations across these seasons depends on the strength of the relevant ice drift curl trend, i.e., autumn sees the strongest anticyclonic ice drift curl trend and the strength of the detrended correlation shows the largest increase. This suggests that the long-term ice drift curl trend is likely playing a significant role in reducing the strength of the trended correlations between the wind and ice drift curl across those
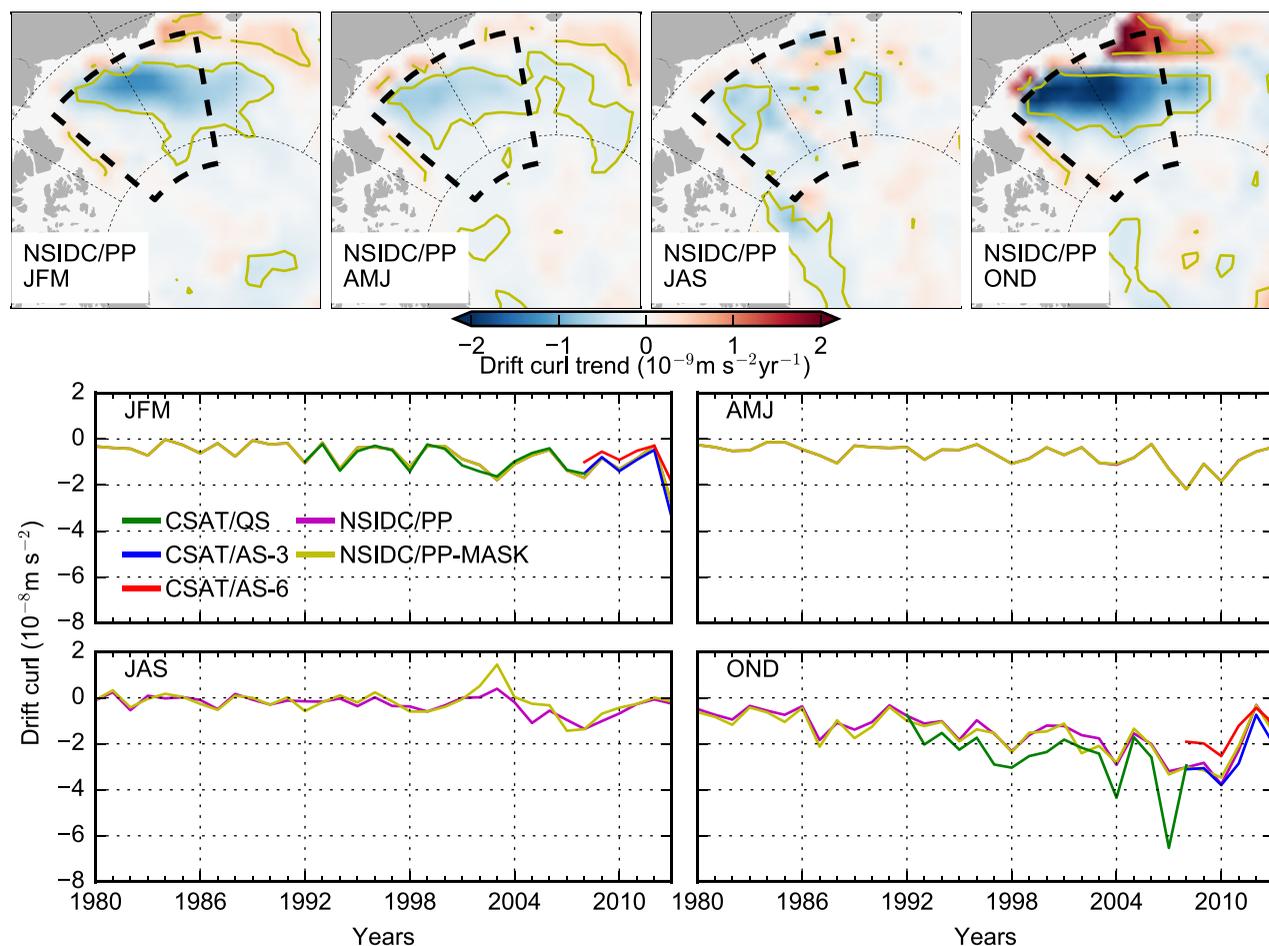
**Figure 9.** (top) Annual trend (1980–2013) in the seasonal mean ice drift curl calculated from the NSIDC/PP drift data (1980–2013). The yellow contour indicates wind curl trends significant at 95% (95%). (bottom) Annual time series of the mean seasonal drift curl within the Beaufort Gyre region (black dashed box, as in Figure 1) using the NSIDC/PP (1980–2013, magenta) CSAT/QS (1992–2008, green), CSAT/AS-6 (2008–2013, red), and CSAT/AS-3 (2008–2013, blue) drift data. The NSIDC/PP-MASK line (1980–2013, yellow) shows the NSIDC/PP drift curl masked based on the minimum drift data areal coverage across the entire temporal range. CSAT ice drift curls are only shown in winter (JFM) and autumn (OND) due to the limited availability of drift data within spring (AMJ) and summer (JAS).

seasons. In summer, the detrended correlation is in-fact slightly lower (0.72–0.74), which suggests that the high trended correlation is in small part due to the anticyclonic trend in both the wind and ice drift.

Figure 7 also shows the temporally evolving difference between the calculated drift curl and the drift curl expected from a linear fit to the wind curl. This idea was described in section 3.2 and is demonstrated graphically in supporting information Figure S2. This shows that across all seasons, the drift curl is less anticyclonic or similar (positive or near zero) to that expected from a linear fit to the winds during the 1980s. This transitions to a more anticyclonic drift curl than expected from a linear fit to the winds (negative value) in the 2000s. The strength of this anticyclonic ice drift curl amplification is strongest in autumn and appears to have increased since the 1980s up to 2010. In spring and summer, however, the strong amplification in ice drift curl occurs mainly between 2007 and 2010.

In spring, summer, and autumn, the ice drift curl is similar to that expected from the winds after 2010. All seasons show a less anticyclonic ice drift in 2012, driven by a near-neutral wind forcing across all seasons. The winter results show a strong anticyclonic ice drift in 2013, coinciding with anomalously anticyclonic winds. The ice circulation, however, is still more anticyclonic than expected from the wind curl, demonstrating the continued potential for an amplified anticyclonic ice drift compared to previous decades.

Supporting information Figure S3 shows the annual mean wind and drift curl, together with the difference between the calculated drift curl and the predicted drift curl assuming a linear fit to the winds, demonstrating a clear ice drift curl amplification between 2008 and 2010.
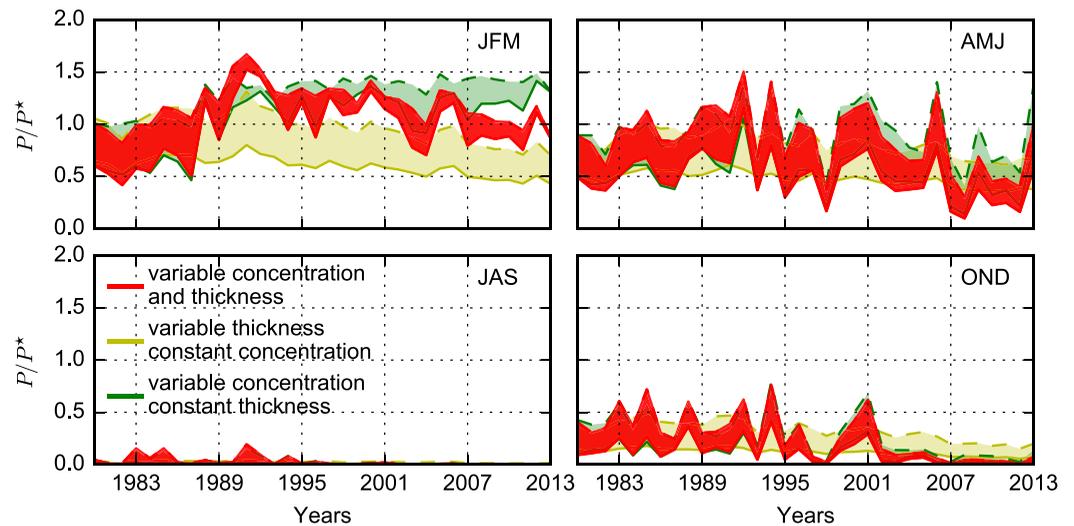
**Figure 10.** Seasonal estimates of ice strength ($P/P^\star$ in equation (9)) in the Beaufort Gyre region (the gray dashed box in Figure 1) from 1980 to 2013, based on monthly estimates of ice concentration (NASA Team and Bootstrap, Figure 4) and thickness (PIOMAS, Figure 5), given by the red shading. The yellow (green) shading show $P/P^\star$ estimated with a constant (1980–1990) seasonal mean concentration (thickness) and variable thickness (concentration). The solid (dashed) lines either side of the shading show the ice strength calculated using the NASA Team (Bootstrap) processing of passive microwave data.

## 5. Discussion

The results presented in the previous section suggest an increased response of the BG ice circulation to wind forcing, especially during the late 2000s. Here we consider potential causes of this amplified ice circulation, which include variations in: the ice interaction force, the atmospheric/oceanic drag coefficients, and the near-surface ocean currents (previously discussed in section 3.2). It is worth noting again that there may be processes not accounted for in our simple model of sea ice momentum transfer, meaning that this discussion is not exhaustive and other processes may be important.

The ice interaction force $\mathbf{F_i}$, introduced in equation (3), is a function of the sea ice strength, which relates the sea ice strain rate to the internal stresses of the ice pack. For large-scale geophysical modeling, sea ice strength is most commonly estimated using the formulation proposed by *Hibler* [1979] as

$$P = P^\star h e^{-C(1-A)} \tag{9}$$

where $h$ is ice thickness, $A$ is ice concentration, and $P^\star$ ($\approx 10^4 - 10^5$ N m$^{-1}$) and $C$ ($\approx$20) are empirical constants [e.g., *Feltham*, 2008]. While this rheology is still used within most state-of-the-art sea ice models, this specific formalism remains poorly validated. For example, *Rothrock* [1975] showed ice strength could be related to $h^2$ based on energetic constraints in pressure ridging, and $P^\star$ is often used as a tunable parameter in sea ice models to match with observed ice dynamics [e.g., *Feltham*, 2008; *Massonnet et al.*, 2014].

To assess the impact of the changing BG ice state on ice strength, Figure 10 shows estimates of the normalized ice strength $P/P^\star$. We normalize the ice strength as $P^\star$ is a highly uncertain parameter, and we are not attempting to quantify the ice strength, but instead seek a qualitative comparison across seasons. A constant value of $C = 20$ is used in all calculations. The ice strength estimates are produced using the seasonal BG ice thickness estimates from PIOMAS data (Figure 3) and ice concentration estimates from both the NASA Team and Bootstrap data (Figure 4). Note that the ice concentration is lower and the seasonal variability is greater in the NASA Team results compared to the Bootstrap results. The estimated linear relationship between ice strength and ice thickness (equation (9)) suggests a weaker impact on ice strength than changes in ice concentration. However, in winter and early spring, when the ice pack remains consolidated, changes in ice thickness are likely to be important. To assess the relative contribution to the estimated ice strength changes from either concentration or thickness, Figure 10 also shows estimates of $P/P^\star$ using constant (1980–1990 seasonal means) concentration or thickness estimates.

In summer, we expect the ice to be near a state of "free drift," when the ice strength and resultant ice interaction force is low/negligible [e.g., *Steele et al.*, 1997]. Indeed we find low values of $P/P^*$ in summer, except for some years where the Bootstrap ice concentration increased over 80% (in the 1980s/1990s). The strong decline in summer ice concentration (∼75–50%) is therefore unlikely to have resulted in much significant change in the pack ice strength. Other processes (as discussed later in this section) are therefore thought to be driving the increased anticyclonic ice drift in summer.

In winter, spring, and especially autumn, the higher mean ice concentration allows for more significant changes in the pack ice strength. Despite the smaller concentration decline in autumn (∼92–82%) compared to summer, the decrease in concentration appears to have pushed the sea ice toward a state of free drift in the 2000s (2002 onward). In spring, the concentration decline caused less of an impact on ice strength than the autumn decrease, although the ice strength is estimated to be lower than average between 2007 and 2012. In spring, the ice thickness decrease has contributed a similar fraction to the decrease in ice strength compared to the concentration decline, albeit with less interannual variability. Interestingly, both spring and autumn show a large decrease in ice strength in 1998, due to decreased ice concentration, which coincide with an amplified ice drift curl in that same year across both seasons (Figure 7).

In winter, both NASA Team and Bootstrap concentration estimates show small increases in ice concentration since the 1980s, resulting in a significant increase in ice strength. Large uncertainties exist in the passive microwave sensing of low winter open water fractions, however [e.g., *Kwok*, 2002], and these winter concentration trends may instead be caused by trends in atmospheric/surface conditions [e.g., *Andersen et al.*, 2007]. The estimated decrease in the winter ice thickness (∼2.5–2 m) implies a decrease in ice strength of similar magnitude to the increase caused by the small change in concentration. The ULS ice thickness estimates are lower than the PIOMAS thickness estimates in the 2000s (autumn and winter), suggesting the contribution from ice thickness changes on ice strength could be higher. It is also worth noting that the big reduction in ice thickness between 2007 and 2008 from PIOMAS and the ULS/IceBridge observations corresponds with the timing of the amplified ice drift curl (Figure 7). *Krishfield et al.* [2014] report a recovery of older ice (greater than 2 m) in 2012 which could be linked to the more cyclonic wind forcing and the lack of ice export through both east-west flux gates in winter 2012.

The spring/autumn concentration declines also suggest a trend toward a concentration that optimizes the transfer of momentum between the atmosphere and ocean, which *Martin et al.* [2014] suggest occurs at a concentration of 80–90%. The decline in ice concentration also lends support to the hypothesis of *Shimada et al.* [2006], that ice is now able to circulate faster through the Beaufort Sea due to reduced coastal shear stresses; a further mechanism through which the strength of the ice interaction force **F_i** may be reduced in spring/autumn. These changes can also be discussed in terms of the length of the melt season within the BG region, with the small trend toward earlier melt onset (in spring) and strong trend toward a later freeze onset (in autumn) [e.g., *Markus et al.*, 2009; *Stroeve et al.*, 2014], potentially extending the period over which the ice remains in free drift.

A further explanation for the enhanced sea ice circulation includes changes in the atmosphere and ocean drag coefficients, $C_a$ and $C_o$, given in equations (4) and (5). These coefficients represent the collective contribution to the total drag on the ice cover from skin drag, a frictional force, and form drag, caused by discrete obstructions to fluid flow from the variable sea ice morphology. While most climate models simply tune a constant skin drag coefficient to account for form drag, a recent modeling study by *Tsamados et al.* [2014] incorporated a variable form drag parameterization scheme into the state-of-the-art sea ice model CICE. They found form drag due to pressure ridges resulted in a small increase (decrease) in the center (southern periphery) of the BG. They also found increased form drag in summer across the BG associated with increased form drag from floe edges (freeboard and draft), highlighting a mechanism through which reductions in low summer ice concentration could further enhance sea ice drift. Inclusion of this new form drag parameterization caused a stronger trend in the curl of the oceanic drag over the BG (compared to assuming a constant atmospheric/oceanic form drag coefficient). However, the new drag parameterizations require considerably more observational constraint before this impact can be reliably quantified.

There has also likely been a decrease in the stability of the atmospheric boundary layer in the Arctic, driven by increases in open water and the resultant increase in the ocean-atmosphere heat flux [e.g., *Schweiger et al.*, 2008]. The stability of the boundary layer is thought to provide a significant impact on atmospheric

drag [e.g., *Andreas et al.*, 1984; *Overland*, 1985], with a less stable boundary layer increasing the effective wind drag on the sea ice cover due to enhanced turbulent mixing. The stability of the Arctic boundary layer shows strong regional and temporal variability, however, and strong disagreements exist between estimates based on reanalyses and observational data [*Boisvert et al.*, 2015]. Reliable long-term estimates of the boundary layer stability and a quantification of the impact of these changes on the atmospheric drag (compared to changes in ice morphology) are needed to assess this possible mechanism of enhanced ice circulation.

The increased doming of the BG [*Giles et al.*, 2012] and associated increases in geostrophic current strength [*McPhee*, 2013] are also contributing to increases in ice drift curl through a reduced ocean-ice stress. Note that the biggest annual increase in SSH in *Giles et al.* [2012] was in 2007/2008, consistent with a period of rapid sea ice loss. *McPhee* [2013] showed strengthening geostrophic currents on the southern periphery of the BG in late summer, which was shown to cause a significant increase in ice drift compared to the ice drift expected from wind forcing alone (assuming free drift). A preliminary analysis extending the BG SSH time series following *Giles et al.* [2012] suggests minimal SSH change since 2010 (up to 2013) [*Armitage et al.*, 2014], which would suggest persistence in the strength of the geostrophic currents. Similarly, an extension of the mean dynamic height analysis in *McPhee* [2013] from 2012 to 2015, suggests persistence in the BG dynamic height and associated geostrophic current strength (M. McPhee, personal communication, 2015). Further research is still needed to elucidate the contribution of ocean forcing to the mean state and interannual/seasonal variability in ice circulation around the BG.

Models used to investigate the BG [e.g., *Proshutinsky and Johnson*, 1997] have demonstrated that the ice/ocean circulation alternates between anticyclonic and cyclonic circulation regimes in response to wind forcing variability. These simplified models, however, do not include the impact of a temporally evolving ice state on momentum transfer from the atmosphere to the ocean, and are unlikely to capture the complex feedbacks associated with ice drift, Ekman transport, and ocean currents. Sophisticated regional ice-ocean models [e.g., *Johnson et al.*, 2007] that also take into account variable ice morphology [*Tsamados et al.*, 2014], momentum transfer [*Martin et al.*, 2014], and SSH variability [e.g., *Koldunov et al.*, 2014] are needed to further investigate the physical drivers of the amplified BG ice circulation presented in this study.

## 6. Summary

We have examined a multidecadal (1980–2013) time series of sea ice drift and wind forcing over the Beaufort Gyre. We find significant (>99%) anticyclonic ice drift trends across all seasons. The strongest anticyclonic ice drift trend is in autumn, associated with an increasing export of ice out of the southern Beaufort Sea (into the Chukchi Sea). Despite these seasonal trends in ice drift curl, a significant (>90%) anticyclonic wind trend occurs in summer only. The seasonal correlations between the wind curl and ice drift curl indicate a strong correlation in summer and winter. Detrended correlations suggest that the long-term ice drift curl trend is playing a significant role in reducing the strength of the correlation between the wind and ice drift curl in autumn (and winter/spring to a lesser extent), while the high correlation in summer is in small part due to the anticyclonic trend in both the wind and ice drift curl. Across all seasons, the ice drift curl is more anticyclonic than expected from the wind curl in the 2000s (~2004 onward) compared to the 1980s/1990s. The strength of this anticyclonic ice drift curl amplification is strongest in autumn and appears to have increased since the 1980s (up to 2010). In spring and summer, however, the strong amplification in ice drift curl occurs mainly between 2007 and 2010. The results also suggest a weakening of the wind and ice circulation (less anticyclonic) since 2010 and return to a circulation regime closer to that observed prior to 2000. Stronger anticyclonic wind forcing, however, still appears able to cause an amplified anticyclonic ice circulation compared to previous decades.

Several mechanisms have been proposed to describe the changing BG ice circulation. Declines in concentration and thickness (which vary seasonally) have likely decreased the BG internal ice strength, reducing the ice interaction force and making the sea ice more mobile. The strong ice drift amplification in autumn has also coincided with a strong trend toward later freezeup within the BG region, extending the period over which the ice pack remains in free drift. Changes to the ice morphology, the atmospheric boundary layer stability, and/or geostrophic currents could also explain the enhanced ice circulation.

The hypotheses presented here are testable in the next generation of regional coupled climate models. This will also enable a quantitative assessment of the various contributions to the enhanced ice circulation, the accumulation of freshwater in the BG between 2002 and 2010 [e.g., *Giles et al.*, 2012], and the probable release of freshwater from the BG over recent years [e.g., *Timmermans et al.*, 2011; *Krishfield et al.*, 2014]. Understanding the wider causes of ice circulation variability around the BG will also increase our understanding of recent and future changes in Arctic sea ice.

# References

Aagaard, K., and E. C. Carmack (1989), The role of sea ice and other fresh water in the Arctic circulation, *J. Geophys. Res.*, *94*(C10), 14,485–14,498, doi:10.1029/JC094iC10p14485.

Andersen, S., R. Tonboe, L. Kaleschke, G. Heygster, and L. T. Pedersen (2007), Intercomparison of passive microwave sea ice concentration retrievals over the high-concentration Arctic sea ice, *J. Geophys. Res.*, *112*, C08004, doi:10.1029/2006JC003543.

Andreas, E. L., W. B. Tucker, and S. F. Ackley (1984), Atmospheric boundary-layer modification, drag coefficient, and surface heat flux in the Antarctic marginal ice zone, *J. Geophys. Res.*, *89*(C1), 649–661, doi:10.1029/JC089iC01p00649.

Armitage, T., D. Wingham, and A. Ridout (2014), Sea level change in the Arctic Ocean from ERS, Envisat and CryoSat-2 radar altimetry, Abstract C11D-02 presented at 2014 Fall Meeting, AGU, San Francisco, Calif.

Asplin, M. G., J. V. Lukovich, and D. G. Barber (2009), Atmospheric forcing of the Beaufort Sea ice gyre: Surface pressure climatology and sea ice motion, *J. Geophys. Res.*, *114*, C00A06, doi:10.1029/2008JC005127.

Boisvert, L. N., D. L. Wu, T. Vihma, and J. Susskind (2015), Verification of air/surface humidity differences from AIRS and ERA-Interim in support of turbulent flux estimation in the Arctic, *J. Geophys. Res. Atmos.*, *120*, 945–963, doi:10.1002/2014JD021666.

Brown, R. A. (1980), Planetary boundary layer modeling for AIDJEX, in *Sea Ice Process and Model*, edited by R. S. Pritchard, pp. 387–401, Univ. of Wash. Press, Seattle.

Cavalieri, D. J., C. L. Parkinson, P. Gloersen, and H. Zwally (1996), Sea ice concentrations from Nimbus-7 SMMR and DMSP SSM/I-SSMIS passive microwave data, NASA DAAC at the Natl. Snow and Ice Data Cent., Boulder, Colo., doi:10.5067/8GQ8LZQVL0VL. [Updated 2014]

Comiso, J. (2000), Bootstrap sea ice concentrations from Nimbus-7 SMMR and DMSP SSM/I-SSMIS. Version 2 [1980-2013], NASA DAAC at the Natl. Snow and Ice Data Cent., Boulder, Colo., doi:10.5067/J6JQLS9EJ5HU. [Updated 2014]

Dee, D. P., et al. (2011), The ERA-Interim reanalysis: configuration and performance of the data assimilation system, *Q. J. R. Meteorol. Soc.*, *137*(656), 553–597, doi:10.1002/qj.828.

Ebita, A., S. Kobayashi, Y. Ota, M. Moriya, R. Kumabe, K. Onogi, Y. Harada, S. Yasui, K. Miyaoka, and K. Takahashi (2011), The Japanese 55-year Reanalysis ''JRA-55'': An interim reports, *SOLA*, *7*, 149–152.

Farrell, S. L., D. C. McAdoo, S. W. Laxon, H. J. Zwally, D. Yi, A. Ridout, and K. Giles (2012), Mean dynamic topography of the Arctic Ocean, *Geophys. Res. Lett.*, *39*, L01601, doi:10.1029/2011GL050052.

Feltham, D. L. (2008), Sea ice rheology, *Annu. Rev. Fluid Mech.*, *40*(1), 91–112, doi:10.1146/annurev.fluid.40.111406.102151.

Fowler, C., W. Emery, and J. Maslanik (2003), Satellite derived Arctic sea ice evolution Oct. 1978 to March 2003, *IEEE Trans. Geosci. Remote Sens. Lett.*, *1*(2), 71–74.

Fowler, C., J. Maslanik, W. Emery, and M. Tschudi (2013), Polar Pathfinder daily 25 km EASE-grid sea ice motion vectors. Version 2. [1980-2013, daily], Natl. Snow and Ice Data Cent., Boulder, Colo.

Giles, K. A., S. W. Laxon, A. L. Ridout, D. J. Wingham, and S. Bacon (2012), Western Arctic Ocean freshwater storage increased by wind-driven spin-up of the Beaufort Gyre, *Nat. Geosci.*, *5*(3), 194–197, doi:10.1038/ngeo1379.

Girard-Ardhuin, F., and R. Ezraty (2012), Enhanced Arctic sea ice drift estimation merging radiometer and scatterometer data, *IEEE Trans. Geosci. Remote Sens.*, *50*(7), 2639–2648, doi:10.1109/TGRS.2012.2184124.

Guest, P. S., and K. L. Davidson (1991), The aerodynamic roughness of different types of sea ice, *J. Geophys. Res.*, *96*(C3), 4709–4721, doi:10.1029/90JC02261.

Hakkinen, S., A. Proshutinsky, and I. Ashik (2008), Sea ice drift in the Arctic since the 1950s, *Geophys. Res. Lett.*, *35*, L19704, doi:10.1029/2008GL034791.

Hibler, W. D. (1979), A dynamic thermodynamic sea ice model, *J. Phys. Oceanogr.*, *9*(4), 815–846, doi:10.1175/1520-0485(1979)009⟨0815:ADTSIM⟩2.0.CO;2.

Hibler, W. D., and K. Bryan (1987), A diagnostic ice-ocean model, *J. Phys. Oceanogr.*, *17*(7), 987–1015, doi:10.1175/1520-0485(1987)017⟨0987:ADIM⟩2.0.CO;2.

Hutchings, J. K., and I. G. Rigor (2012), Role of ice dynamics in anomalous ice conditions in the Beaufort Sea during 2006 and 2007, *J. Geophys. Res.*, *117*, C00E04, doi:10.1029/2011JC007182.

Jakobsson, M., et al. (2012), The International Bathymetric Chart of the Arctic Ocean (IBCAO) Version 3.0, *Geophys. Res. Lett.*, *39*, L12609, doi:10.1029/2012GL052219.

Johnson, M., S. Gaffigan, E. Hunke, and R. Gerdes (2007), A comparison of Arctic Ocean sea ice concentration among the coordinated AOMIP model experiments, *J. Geophys. Res.*, *112*, C04S11, doi:10.1029/2006JC003690.

Kanamitsu, M., W. Ebisuzaki, J. Woollen, S.-K. Yang, J. J. Hnilo, M. Fiorino, and G. L. Potter (2002), NCEP-DOE AMIP-II Reanalysis (R-2), *Bull. Am. Meteorol. Soc.*, *83*(11), 1631–1643, doi:10.1175/BAMS-83-11-1631.

Koldunov, N. V., et al. (2014), Multimodel simulations of Arctic Ocean sea surface height variability in the period 1970–2009, *J. Geophys. Res. Oceans*, *119*, 8936–8954, doi:10.1002/2014JC010170.

Krishfield, R. A., A. Proshutinsky, K. Tateyama, W. J. Williams, E. C. Carmack, F. A. McLaughlin, and M.-L. Timmermans (2014), Deterioration of perennial sea ice in the Beaufort Gyre from 2003 to 2012 and its impact on the oceanic freshwater cycle, *J. Geophys. Res. Oceans*, *119*, 1271–1305, doi:10.1002/2013JC008999.

Kwok, R. (2002), Sea ice concentration estimates from satellite passive microwave radiometry and openings from SAR ice motion, *Geophys. Res. Lett.*, *29*(9), 1311, doi:10.1029/2002GL014787.

Kwok, R., and G. F. Cunningham (2010), Contribution of melt in the Beaufort Sea to the decline in Arctic multiyear sea ice coverage: 1993-2009, *Geophys. Res. Lett.*, *37*, L20501, doi:10.1029/2010GL044678.

Kwok, R., G. Spreen, and S. Pang (2013), Arctic sea ice circulation and drift speed: Decadal trends and ocean currents, *J. Geophys. Res. Oceans*, *118*, 2408–2425, doi:10.1002/jgrc.20191.

Lindsay, R., and A. Schweiger (2015), Arctic sea ice thickness loss determined using subsurface, aircraft, and satellite observations, *The Cryosphere*, *9*(1), 269–283.

Lindsay, R., M. Wensnahan, A. Schweiger, and J. Zhang (2014), Evaluation of seven different atmospheric reanalysis products in the Arctic*, *J. Clim.*, *7*(7), 2588–2606, doi:10.1175/JCLI-D-13-00014.1.

Lupkes, C., V. M. Gryanik, J. Hartmann, and E. L. Andreas (2012), A parametrization, based on sea ice morphology, of the neutral atmospheric drag coefficients for weather prediction and climate models, *J. Geophys. Res.*, *117*, D13112, doi:10.1029/2012JD017630.

Markus, T., J. C. Stroeve, and J. Miller (2009), Recent changes in Arctic sea ice melt onset, freezeup, and melt season length, *J. Geophys. Res.*, *114*, C12024, doi:10.1029/2009JC005436.

Martin, T., M. Steele, and J. Zhang (2014), Seasonality and long-term trend of Arctic Ocean surface stress in a model, *J. Geophys. Res. Oceans*, *119*, 1723–1738, doi:10.1002/2013JC009425.

Maslanik, J., S. Drobot, C. Fowler, W. Emery, and R. Barry (2007), On the Arctic climate paradox and the continuing role of atmospheric circulation in affecting sea ice conditions, *Geophys. Res. Lett.*, *34*, L03711, doi:10.1029/2006GL028269.

Maslanik, J., J. Stroeve, C. Fowler, and W. Emery (2011), Distribution and trends in Arctic sea ice age through spring 2011, *Geophys. Res. Lett.*, *38*, L13502, doi:10.1029/2011GL047735.

Massonnet, F., H. Goosse, T. Fichefet, and F. Counillon (2014), Calibration of sea ice dynamic parameters in an ocean-sea ice model using an ensemble Kalman filter, *J. Geophys. Res. Oceans*, *119*, 4168–4184, doi:10.1002/2013JC009705.

McPhee, M. G. (1982), Sea ice drag laws and simple boundary layer concepts, including application to rapid melting, *CRREL Rep. 82-4*, *Tech. Rep. 17*, U.S. Army Cold Reg. Res. and Eng. Lab., Hanover, N. H.

McPhee, M. G. (2012), Advances in understanding ice-ocean stress during and since AIDJEX, *Cold Reg. Sci. Technol.*, *76-77*, 24–36, doi: 10.1016/j.coldregions.2011.05.001.

McPhee, M. G. (2013), Intensification of geostrophic currents in the Canada Basin, Arctic Ocean, *J. Clim.*, *26*(10), 3130–3138, doi:10.1175/JCLI-D-12-00289.1.

McPhee, M. G., A. Proshutinsky, J. H. Morison, M. Steele, and M. B. Alkire (2009), Rapid change in freshwater content of the Arctic Ocean, *Geophys. Res. Lett.*, *36*, L10602, doi:10.1029/2009GL037525.

Morison, J., R. Kwok, C. Peralta-Ferriz, M. Alkire, I. Rigor, R. Andersen, and M. Steele (2012), Changing Arctic Ocean freshwater pathways, *Nature*, *481*(7379), 66–70, doi:10.1038/nature10705.

Overland, J. E. (1985), Atmospheric boundary layer structure and drag coefficients over sea ice, *J. Geophys. Res.*, *90*(C5), 9029–9049.

Parkinson, C. L., and J. C. Comiso (2013), On the 2012 record low Arctic sea ice cover: Combined impact of preconditioning and an August storm, *Geophys. Res. Lett.*, *40*, 1356–1361, doi:10.1002/grl.50349.

Perovich, D. K., J. A. Richter-Menge, K. F. Jones, and B. Light (2008), Sunlight, water, and ice: Extreme Arctic sea ice melt during the summer of 2007, *Geophys. Res. Lett.*, *35*, L11501, doi:10.1029/2008GL034007.

Perovich, D. K., K. F. Jones, B. Light, H. Eicken, T. Markus, J. Stroeve, and R. Lindsay (2011), Solar partitioning in a changing Arctic sea-ice cover, *Ann. Glaciol.*, *52*(57), 192–196, doi:10.3189/172756411795931543.

Proshutinsky, A., R. H. Bourke, and F. A. McLaughlin (2002), The role of the Beaufort Gyre in Arctic climate variability: Seasonal to decadal climate scales, *Geophys. Res. Lett.*, *29*(23), 2100, doi:10.1029/2002GL015847.

Proshutinsky, A., R. Krishfield, M.-L. Timmermans, J. Toole, E. Carmack, F. McLaughlin, W. J. Williams, S. Zimmermann, M. Itoh, and K. Shimada (2009), Beaufort Gyre freshwater reservoir: State and variability from observations, *J. Geophys. Res.*, *114*, C00A10, doi: 10.1029/2008JC005104.

Proshutinsky, A. Y., and M. A. Johnson (1997), Two circulation regimes of the wind-driven Arctic Ocean, *J. Geophys. Res.*, *102*(C6), 12,493–12,514, doi:10.1029/97JC00738.

Rabe, B., M. Karcher, U. Schauer, J. M. Toole, R. A. Krishfield, S. Pisarev, F. Kauker, R. Gerdes, and T. Kikuchi (2011), An assessment of Arctic Ocean freshwater content changes from the 1990s to the 2006-2008 period, *Deep Sea Res., Part I*, *58*(2), 173–185, doi:10.1016/j.dsr.2010.12.002.

Rampal, P., J. Weiss, and D. Marsan (2009), Positive trend in the mean speed and deformation rate of Arctic sea ice, 1979-2007, *J. Geophys. Res.*, *114*, C05013, doi:10.1029/2008JC005066.

Richter-Menge, J. A., and S. L. Farrell (2013), Arctic sea ice conditions in spring 2009-2013 prior to melt, *Geophys. Res. Lett.*, *40*, 5888–5893, doi:10.1002/2013GL058011.

Rigor, I. G., and J. M. Wallace (2004), Variations in the age of Arctic sea-ice and summer sea-ice extent, *Geophys. Res. Lett.*, *31*, L09401, doi: 10.1029/2004GL019492.

Rigor, I. G., J. M. Wallace, and R. L. Colony (2002), Response of sea ice to the Arctic Oscillation, *J. Clim.*, *15*(18), 2648–2663, doi:10.1175/1520-0442(2002)015⟨2648:ROSITT⟩2.0.CO;2.

Rothrock, D. A. (1975), The energetics of the plastic deformation of pack ice by ridging, *J. Geophys. Res.*, *80*(33), 4514–4519, doi:10.1029/JC080i033p04514.

Rothrock, D. A., D. B. Percival, and M. Wensnahan (2008), The decline in arctic sea-ice thickness: Separating the spatial, annual, and interannual variability in a quarter century of submarine data, *J. Geophys. Res.*, *113*, C05003, doi:10.1029/2007JC004252.

Schweiger, A., R. Lindsay, J. Zhang, M. Steele, H. Stern, and R. Kwok (2011), Uncertainty in modeled Arctic sea ice volume, *J. Geophys. Res.*, *116*, C00D06, doi:10.1029/2011JC007084.

Schweiger, A. J., R. W. Lindsay, S. Vavrus, and J. A. Francis (2008), Relationships between Arctic sea ice and clouds during autumn, *J. Clim.*, *21*(18), 4799–4810, doi:10.1175/2008JCLI2156.1.

Screen, J. A., I. Simmonds, and K. Keay (2011), Dramatic interannual changes of perennial Arctic sea ice linked to abnormal summer storm activity, *J. Geophys. Res.*, *116*, D15105, doi:10.1029/2011JD015847.

Serreze, M. C., and A. P. Barrett (2010), Characteristics of the Beaufort Sea High, *J. Clim.*, *24*(1), 159–182, doi:10.1175/2010JCLI3636.1.

Shimada, K., T. Kamoshida, M. Itoh, S. Nishino, E. Carmack, F. McLaughlin, S. Zimmermann, and A. Proshutinsky (2006), Pacific Ocean inflow: Influence on catastrophic reduction of sea ice cover in the Arctic Ocean, *Geophys. Res. Lett.*, *33*, L08605, doi:10.1029/2005GL025624.

Spreen, G., R. Kwok, and D. Menemenlis (2011), Trends in Arctic sea ice drift and role of wind forcing: 1992-2009, *Geophys. Res. Lett.*, *38*, L19501, doi:10.1029/2011GL048970.

Steele, M., J. Zhang, D. Rothrock, and H. Stern (1997), The force balance of sea ice in a numerical model of the Arctic Ocean, *J. Geophys. Res.*, *102*(C9), 21,061–21,079, doi:10.1029/97JC01454.

Stroeve, J. C., J. Maslanik, M. C. Serreze, I. Rigor, W. Meier, and C. Fowler (2011), Sea ice response to an extreme negative phase of the Arctic Oscillation during winter 2009/2010, *Geophys. Res. Lett.*, *38*, L02502, doi:10.1029/2010GL045662.

Stroeve, J. C., T. Markus, L. Boisvert, J. Miller, and A. Barrett (2014), Changes in Arctic melt season and implications for sea ice loss, *Geophys. Res. Lett.*, *41*, 1216–1225, doi:10.1002/2013GL058951.

Sumata, H., T. Lavergne, F. Girard-Ardhuin, N. Kimura, M. A. Tschudi, F. Kauker, M. Karcher, and G. Rudiger (2014), An intercomparison of Arctic ice drift products to deduce uncertainty estimates, *J. Geophys. Res. Oceans*, 119, 4887–4921, doi:10.1002/2013JC009724.

Thorndike, A. S., and R. Colony (1982), Sea ice motion in response to geostrophic winds, *J. Geophys. Res.*, 87(C8), 5845–5852, doi:10.1029/JC087iC08p05845.

Timmermans, M.-L., A. Proshutinsky, R. A. Krishfield, D. K. Perovich, J. A. Richter-Menge, T. P. Stanton, and J. M. Toole (2011), Surface freshening in the Arctic Ocean's Eurasian Basin: An apparent consequence of recent change in the wind-driven circulation, *J. Geophys. Res.*, 116, C00D03, doi:10.1029/2011JC006975.

Tsamados, M., D. L. Feltham, D. Schroeder, D. Flocco, S. L. Farrell, N. Kurtz, S. W. Laxon, and S. Bacon (2014), Impact of variable atmospheric and oceanic form drag on simulations of Arctic sea ice, *J. Phys. Oceanogr.*, 44, 1329–1353, doi:10.1175/JPO-D-13-0215.1.

Warren, S. G., I. G. Rigor, N. Untersteiner, V. F. Radionov, N. N. Bryazgin, Y. I. Aleksandrov, and R. Colony (1999), Snow depth on arctic sea ice, *J. Clim.*, 12(6), 1814–1829, doi:10.1175/1520-0442(1999)012⟨1814:SDOASI⟩2.0.CO;2.

Webster, M. A., I. G. Rigor, S. V. Nghiem, N. T. Kurtz, S. L. Farrell, D. K. Perovich, and M. Sturm (2014), Interdecadal changes in snow depth on Arctic sea ice, *J. Geophys. Res. Oceans*, 119, 5395–5406, doi:10.1002/2014JC009985.

Yamamoto-Kawai, M., F. A. McLaughlin, E. C. Carmack, S. Nishino, K. Shimada, and N. Kurita (2009), Surface freshening of the Canada Basin, 2003-2007: River runoff versus sea ice meltwater, *J. Geophys. Res.*, 114, C00A05, doi:10.1029/2008JC005000.

Yang, J. (2009), Seasonal and interannual variability of downwelling in the Beaufort Sea, *J. Geophys. Res.*, 114, C00A14, doi:10.1029/2008JC005084.